Supporting Information

Acid-Induced Mixed Electron and Proton Conduction in Thin ZrO_2 Films

John R. Swierk,[1,*] Nicholas S. McCool,[2] Jason A. Röhr,[1] Svante Hedström,[1,†] Steven J. Konezny,[1,*] Coleen T. Nemes,[1] Pengtao Xu,[2] Victor S. Batista,[1,*] Thomas E. Mallouk,[2,3,*] Charles A. Schmuttenmaer[1,*]

1. Department of Chemistry and Energy Sciences Institute, Yale University, 225 Prospect Street, P.O. Box 208107, New Haven, Connecticut, 06520-8107, United States

2. Department of Chemistry, The Pennsylvania State University, University Park, Pennsylvania 16802 United States

3. Department of Biochemistry and Molecular Biology and Department of Physics, The Pennsylvania State University, University Park, Pennsylvania 16802 United States

†Current address: Department of Physics, Albanova University Center, Stockholm University, 10691 Stockholm, Sweden

EXPERIMENTAL METHODS

Bis(2,2′-bipyridine)(4,4′-diphosphonato-2,2′-bipyridine)ruthenium(II) bromide (Ru(II)phos) was prepared as previously described.[1]

Sample Preparation. ZrO_2 films were fabricated using a Cambridge Savannah 200 ALD system. Vapor pulses were held in the reaction chamber for 3 minutes followed by opening the valve and purging with N_2 for 25 seconds before the next pulse. Tetrakis(dimethylamido)zirconium was used as a precursor with a deposition temperature of 200 °C and a precursor temperature of 75 °C. The pulse durations for this material were 0.015 s and 0.25 s for the water vapor and ZrO_2 precursor, respectively. . The deposition rate for this precursor is commercially reported to be 1.02 Å per cycle at 200 °C on a Si wafer, which agrees well with our ellipsometric measurements on a silicon wafer. Films ranging from 0 to 40 Å were grown on mesoporous, nanoparticulate SnO_2 and from 0 to 200 Å on planar sapphire substrates. ALD is a well-established technique for growing conformal, pinhole-free layers on mesoporous substrates.[2,3] Following shell deposition, all films were annealed at 450 °C for 30 min. Dye-sensitized samples were sensitized in the dark from a 100 μM solution of Ru(II)phos in anhydrous ethanol for 16 hours.

The preparation of high surface area, nanoparticulate SnO_2 films on fused quartz substrates for time-resolved THz spectroscopy (TRTS) measurements are described in detail elsewhere.[4] Briefly, the films were prepared by doctor-blading a SnO_2 paste on fused quartz substrates using Scotch Magic tape as a spacer layer and then sintering at 470 °C. Samples for TRTS were sealed using a second piece of fused quartz separated with a 60 μm Surlyn (Solaronix) spacer between the two pieces of quartz and filled with 0.1 M $HClO_4$(aq) or 0.1 M $LiClO_4$ in acetonitrile, as described in the text.

Scanning/transmission electron microscopy and energy-dispersive X-ray spectroscopy was carried out on an FEI Talos F200X S/TEM instrument. XPS was carried out on a PHI *VersaProbe* II Scanning XPS Microprobe.

Conductivity Measurements. Gold electrical top contacts with a chromium adhesion layer were deposited onto 4 and 20 nm ZrO_2 films on sapphire by physical vapor deposition (Figure S1). The conductivity was obtained from current-voltage characteristics in the range of 0 to 10 V with an Agilent B1500A semiconductor device analyzer equipped with medium-power source-measurement units that use atto-sense and switch units for high-resolution current sensing. Samples were mounted on a triaxially grounded sample stage inside a vacuum chamber. Humid atmosphere conditions were achieved by saturating the vent valve screen attached to the inlet port of the vacuum pump with either water or D_2O ($p_{H2O} = 0.012 \pm 0.003$ atm) just prior to venting the system with ambient air ($p_{H2O} \sim 0.007$ atm). Acid-treated samples were soaked after electrode deposition for a minimum of 8 hours in 0.1 M $HClO_4$ prior to electrical measurements.

TRTS Measurements. Specific details for OPTP measurements are described in detail elsewhere.[5-6] OPTP scans are obtained by measuring the change in THz pule amplitude (ΔTHz) resulting from photoexcitation with 400 nm light as a function of optical-pump THz-probe time delay.

The TRTS scans were fit using the following function:

$$\Delta THz = -\left\{\sum_{i=1}^{n} A_i\left[\exp\left(-\frac{t-t_0}{\tau_i}\right)-1\right]\right\}\otimes G(FWHM) \quad \text{(S1)}$$

where n is the number of exponentials included in the fit, t_0 corresponds to arrival time of the photoexcitation pulse (i.e., t=0), A_i is the amplitude of a given component, τ_i is the lifetime of a given component, G(FWHM) is a Gaussian instrument response function with a full-width at half-maximum of 0.5 ps, and ä„ represents a convolution.

Quantum chemistry calculations. Density functional theory (DFT) calculations using the Gaussian09[7] software at the B3LYP/Def2TZVP//Def2SVP[8] level of theory were performed on the ester form of Ru(II)Phos in implicit CH_3CN,[9] and the acid form in H_2O, respectively. The ground state, S_0, first triplet excited state, T_1, and singly oxidized state, were optimized with unrestricted DFT (uDFT) with the Def2SVP basis set.[10] The first excited singlet state, S_1, was optimized with linear-response time-dependent (TD) DFT with the Def2SVP basis set. At each of the four resulting geometries (optimized S_0, S_1, T_1, and Ox. geometries), single point energy calculations were performed for all electronic configurations, yielding in total 16 points on four potential energy surfaces (PES). The single point calculations were done with the Def2TZVP basis set except for S_1 where the Def2SVP basis set was used. The experimental oxidation potential was obtained from voltammetry measurements of the esterified form of Ru(II)phos in a CH_3CN solvent, so corresponding calculations in the same solvent were performed on the ground and oxidized states at the same level of theory. Calculated potentials vs NHE were obtained by assuming an NHE potential of 4.44 V vs vacuum.[11]

The electron transmission $T(E)$ through the ZrO_2 was modeled with the WKB approximation:

$$T(E) = e^{-2\int_0^d \sqrt{\frac{2m|E-\xi(x)|}{\hbar^2}}dx} = e^{-2d\sqrt{\frac{2m|E-\xi|}{\hbar^2}}} \quad \text{(S2)}$$

with barrier widths d and electron mass m. ξ is taken as the excited state potential of Ru(II)Phos and E as the CBM of ZrO_2.

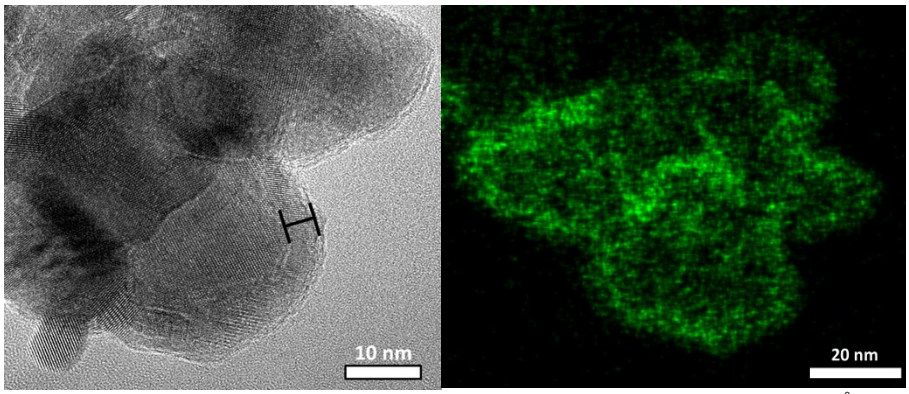

Figure S1. *(Left)* High resolution TEM image of particles from a SnO_2/40p ZrO_2 (~40 Å) nanoparticle film after use in TRTS experiments. Brackets identify ZrO_2 film on the SnO_2 core *(Right)* Representative energy dispersive X-ray spectroscopy map image of 40 pulse cycles (~40 Å) of ZrO_2 coated on SnO_2 nanoparticles (collected after TRTS measurements). Zr is colored green and is seen to uniformly coat the SnO_2 particles.

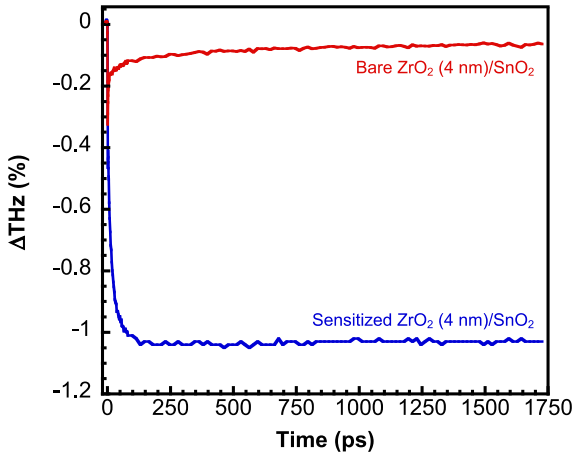

Figure S2. TRTS electron injection for Ru(II)phos-sensitized and bare SnO_2 covered with a 40 Å ZrO_2 film sealed in 0.1 M $HClO_4$.

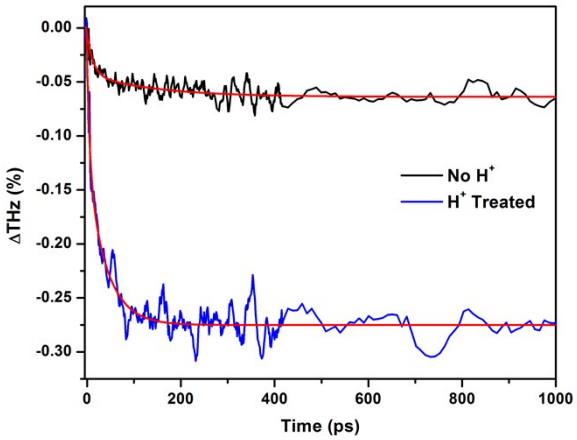

Figure S3: TRTS electron injection for Ru(II)phos-sensitized ZrO_2(40 Å)/SnO_2, measured in acetonitrile with 0.1 M $LiClO_4$. The H^+-treated sample was exposed to 0.1 M $HClO_4$ overnight, rinsed with water and dried before being sealed with the acetonitrile solution.

Table S1. Fitting Parameters for SnO_2/ZrO_2 core/shell structures from Figure 3a.

Shell Thickness [Å]	A_1 [%]	τ_1 [ps]	A_2 [%]	τ_2 [ps]	A_3 (%)	τ_3 [ps]	A_4 [%]	τ_4 [ps]	scaling factor	$<\tau_w>$ [ps]
0	0.20	1.1	0.58	7.5	0.22	38	-0.55	9644	1.32	17
1.02	0.36	2.8	0.52	12	0.12	67			1.45	16
2.04	0.39	2.8	0.49	15	0.12	103			1.62	21
2.04	0.39	2.7	0.49	14	0.12	107			1.67	20
5.10	0.38	2.8	0.46	17	0.16	101			1.16	25
5.10	0.42	3.2	0.46	16	0.11	106			1.21	21
10.2	0.38	3.1	0.47	17	0.15	127			0.90	28
10.2	0.61	5.2	0.24	24	0.16	277			0.71	52
20.4	0.30	2.8	0.54	14	0.16	111			0.70	26
20.4	0.45	3.6	0.44	16	0.12	98			0.68	20
40.8	0.32	2.8	0.50	20	0.18	227			0.62	52
40.8	0.26	2.4	0.47	18	0.27	209			0.42	66

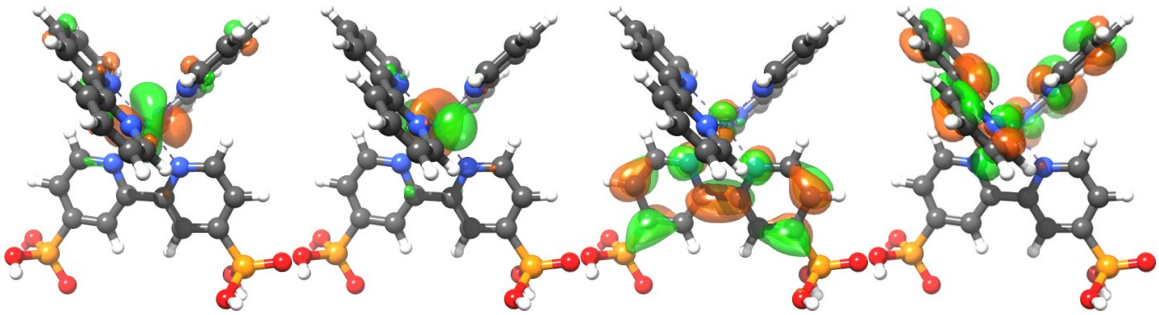

Figure S4. Isodensity plots (isovalue=0.035) of HOMO−1, HOMO, LUMO, and LUMO+1 of the Ru(II)phos dye in its ground state, as calculated at the B3LYP/Def2TZVP//Def2SVP level of theory in a water implicit solvent.

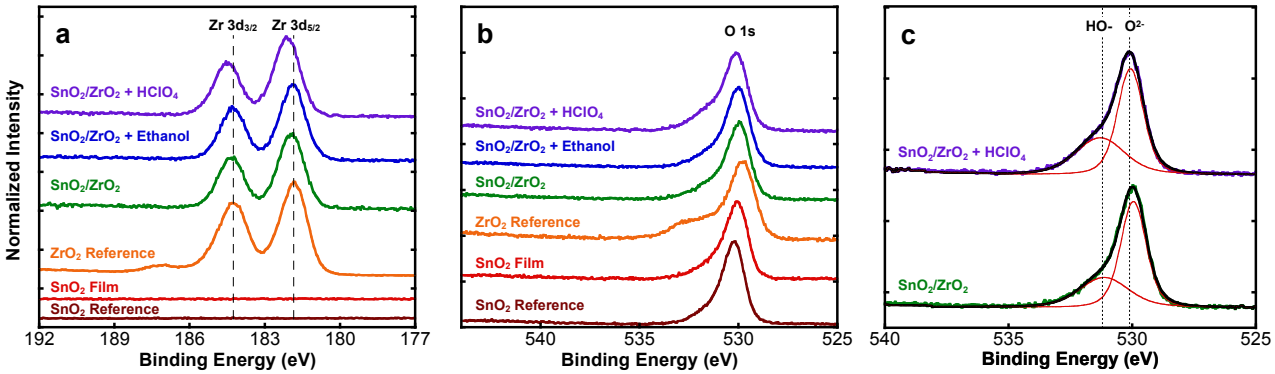

Figure S5. a) Zr 3*d* and b) O 1*s* X-ray photoelectron spectra of commercial SnO_2 and ZrO_2 powders, an SnO_2 film made from the commercial powder, as-prepared SnO_2/ZrO_2 (40 Å) film, and SnO_2/ZrO_2 (40 Å) films that had been exposed to either ethanol or 0.1 M $HClO_4$ overnight. All film samples were mechanically scraped up into a powder for analysis. c) Constrained fitting of the O 1*s* spectra for as-prepared SnO_2/ZrO_2 and acid-treated SnO_2/ZrO_2. The acid treated sample exhibits an increased ratio of hydroxyl oxygen to bridging oxygen (0.7:1) as compared to the as-prepared material (0.52:1).

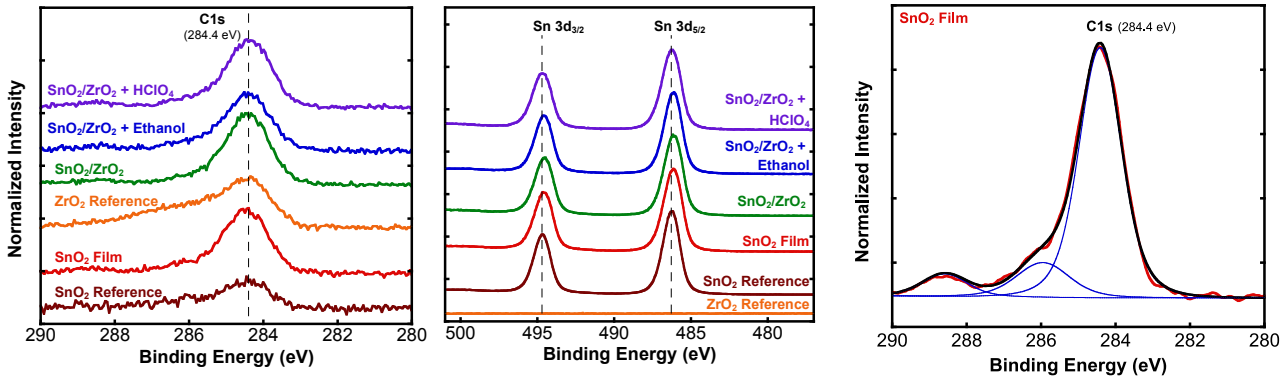

Figure S6. (*Left*) C 1*s* and (*middle*) Sn 3*d* X-ray photoelectron spectra of commercial SnO_2 and ZrO_2 powders, an SnO_2 film made from the commercial powder, as-prepared SnO_2/ZrO_2 (40 Å) film, and SnO_2/ZrO_2 (40 Å) films that had been exposed to either ethanol or 0.1 M $HClO_4$ overnight. All film samples were mechanically scraped from the quartz substrates into a powder for analysis. (*Right*) Experimental XPS spectrum of SnO_2 film (red) and XPS spectrum (black) generated from a fit with three components (blue) to show features at 284.4, 286, and 288.5 eV.

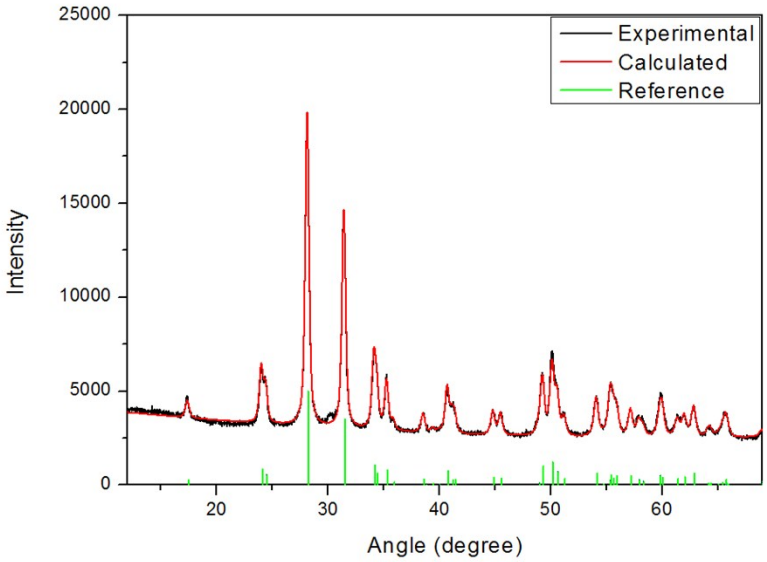

Figure S7. X-ray diffraction pattern for ZrO_2 reference powder (black, experimental) with Rietveld refinement (red) of the monoclinic ZrO_2 reference pattern (green, JCPDS 98-000-0105).[12]

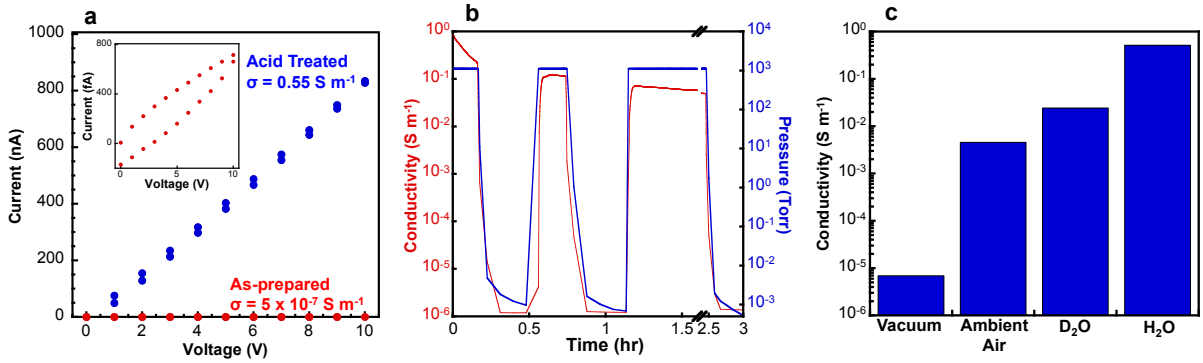

Figure S8. a) Current versus applied potential (I–V) for 40 Å ZrO_2 films on sapphire patterned with interdigitated gold electrodes. Acid-treated film soaked in 0.1 M $HClO_4$ (*aq*) for 18 hours. (*Inset)* The I–V curve for as-prepared ZrO_2. b) Conductivity of an acid-treated 40 Å ZrO_2 film as a function of pressure in ambient atmosphere. c) Conductivity of an acid-treated 40 Å ZrO_2 film in vacuum, ambient air, D_2O-humidified air, and H_2O-humidified air.

References

(1) Gillaizeau-Gauthier, I.; Odobel, F.; Alebbi, M.; Argazzi, R.; Costa, E.; Bignozzi, C. A.; Qu, P.; Meyer, G. J. Phosphonate-Based Bipyridine Dyes for Stable Photovoltaic Devices. *Inorg. Chem.* **2001**, *40* (23), 6073–6079.

(2) Prasittichai, C.; Avila, J. R.; Farha, O. K.; Hupp, J. T. Systematic Modulation of Quantum (Electron) Tunneling Behavior by Atomic Layer Deposition on Nanoparticulate SnO2 and TiO2 Photoanodes. *J. Am. Chem. Soc.* **2013**, *135* (44), 16328–16331.

(3) Lapides, A. M.; Sherman, B. D.; Brennaman, M. K.; Dares, C. J.; Skinner, K. R.; Templeton, J. L.; Meyer, T. J. Synthesis, Characterization, and Water Oxidation by a Molecular Chromophore-Catalyst Assembly Prepared by Atomic Layer Deposition. The "Mummy" Strategy. *Chem. Sci.* **2015**, *6* (11), 6398–6406.

(4) Swierk, J. R.; McCool, N. S.; Nemes, C. T.; Mallouk, T. E.; Schmuttenmaer, C. A. Ultrafast Electron Injection Dynamics of Photoanodes for Water-Splitting Dye-Sensitized Photoelectrochemical Cells. *J. Phys. Chem. C* **2016**, *120*, 5940–5948.

(5) Beard, M. C.; Turner, G. M.; Schmuttenmaer, C. A. Transient Photoconductivity in GaAs as Measured by Time-Resolved Terahertz Spectroscopy. Phys. Rev. B 2000, 62, 15764–15777.

(6) Nemes, C. T.; Koenigsmann, C.; Schmuttenmaer, C. A. Functioning Photoelectrochemical Devices Studied with Time-Resolved Terahertz Spectroscopy. *J. Phys. Chem. Lett.* **2015**, *6* (16), 3257–3262.

(7) Gaussian 09, Revision D.01, M. J. Frisch, G. W. Trucks, H. B. Schlegel, G. E. Scuseria, M. A. Robb, J. R. Cheeseman, G. Scalmani, V. Barone, G. A. Petersson, H. Nakatsuji, X. Li, M. Caricato, A. Marenich, J. Bloino, B. G. Janesko, R. Gomperts, B. Mennucci, H. P. Hratchian, J. V. Ortiz, A. F. Izmaylov, J. L. Sonnenberg, D. Williams-Young, F. Ding, F. Lipparini, F. Egidi, J. Goings, B. Peng, A. Petrone, T. Henderson, D. Ranasinghe, V. G. Zakrzewski, J. Gao, N. Rega, G. Zheng, W. Liang, M. Hada, M. Ehara, K. Toyota, R. Fukuda, J. Hasegawa, M. Ishida, T.

Nakajima, Y. Honda, O. Kitao, H. Nakai, T. Vreven, K. Throssell, J. A. Montgomery, Jr., J. E. Peralta, F. Ogliaro, M. Bearpark, J. J. Heyd, E. Brothers, K. N. Kudin, V. N. Staroverov, T. Keith, R. Kobayashi, J. Normand, K. Raghavachari, A. Rendell, J. C. Burant, S. S. Iyengar, J. Tomasi, M. Cossi, J. M. Millam, M. Klene, C. Adamo, R. Cammi, J. W. Ochterski, R. L. Martin, K. Morokuma, O. Farkas, J. B. Foresman, and D. J. Fox, Gaussian, Inc., Wallingford CT, 2016.

(8) Becke, A. D. Density-Functional Thermochemistry. III. the Role of Exact Exchange. *J. Chem. Phys.* **1993**, *98* (7), 5648–5652.

(9) Marenich, A. V.; Cramer, C. J.; Truhlar, D. G. Universal Solvation Model Based on Solute Electron Density and on a Continuum Model of the Solvent Defined by the Bulk Dielectric Constant and Atomic Surface Tensions. *J. Phys. Chem. B* **2009**, *113* (18), 6378–6396.

(10) Weigend, F.; Ahlrichs, R. Balanced Basis Sets of Split Valence, Triple Zeta Valence and Quadruple Zeta Valence Quality for H to Rn: Design and Assessment of Accuracy. *Phys. Chem. Chem. Phys.* **2005**, *7* (18), 3297–3305.

(11) IUPAC. Standard Hydrogen Electrode. In IUPAC Compendium of Chemical Terminology; IUPAC: Research Triangle Park, NC.

(12) Smith, D. K. and Newkirk, H. W. The Crystal Structure of Baddeleyite (Monoclinic ZrO_2) and its Relation to the Polymorphism of ZrO_2. *Acta Cryst.* **1965**, *18*, 983-991.